Collisionless collective modes of fermions in magnetic traps

P. Capuzzi and E. S. Hernández*

Departamento de Física, Facultad de Ciencias Exactas y Naturales, Universidad de Buenos Aires, RA-1428 Buenos Aires, Argentina

We present a random-phase-approximation formalism for the collective spectrum of two hyperfine species of dilute ^{40}K atoms, magnetically trapped at zero temperature and subjected to a repulsive s-wave interaction between atoms with different spin projections. We examine the density and the spin oscillation spectra, as well as the transition density profiles created by external multipolar fields. The zero sound spectrum is always fragmented and the density and spin channels become clearly distinguishable if the trapping potentials acting on the species are identical. Although this distinction is lost when these confining fields are different, at selected excitation frequencies the transition densities may display the signature of the channel.

I. INTRODUCTION

The realization of Bose-Einstein condensation of alkali-metal atoms in magnetic traps triggered substantial experimental efforts, aimed at cooling fermion isotopes below their Fermi temperatures. In particular, lithium and potassium have been trapped and cooled [1–3], and a recent experiment displays unambiguous evidence of quantum degeneracy effects at temperatures around half the Fermi temperature of ^{40}K atoms [4] in a harmonic trap. On the other hand, various theoretical descriptions of thermodynamical properties of confined, cool free fermions have been presented, either in the semiclassical limit [5] or with explicit consideration of quantum shell effects [6]. In Ref. [7], a Hartree-Fock (HF) calculation of the mean-field spectrum of two hyperfine fermionic species subjected to s-wave attraction has been forwarded. Moreover, in view of the presence of both fermion and boson isotopes in natural alkali-metal samples, the consequences of their coexistence and mutual coupling at zero temperature in the magnetic trap are a topic of current interest [8–13], as well as the possible occurrence of BCS-like superfluid states driven by attractive interactions [14–19].

An important step towards a full understanding of the behavior of coexisting hyperfine species is the knowledge of their collective excitation spectrum. In this context, the collisionless modes of an extended system with various hyperfine levels have been examined in the frame of Landau's theory of Fermi liquids [20], and the zero-sound collective spectra of two species of confined fermions have been computed resorting to sum rules [21]. Assuming local equilibrium of a Fermi gas, described by a Thomas-Fermi (TF) approximation, the linearized hydrodynamic equations can be analytically solved both in the degenerate and in the classical limits [22]. A related hydrodynamic approach based on the equations of motion for the first and second moments of the fermionic Wigner distribution allowed us to compute the oscillation modes of an isotope with one- [23] and two-spin components [24]. More recently, an interacting, quantum degenerate Fermi gas of ^{40}K atoms in two-spin states has been

experimentally produced [25].

Since the two hyperfine species of trapped fermionic atoms are very dilute, it is not clear that when the system is excited by a low-frequency external field, the s-wave interaction—which is supposed to play a relevant role in thermalization during the evaporative cooling process—may permit the trapped gas to equilibrate locally and develop hydrodynamic oscillation modes. In particular, it has been shown that for ^{40}K, at least 10^8 atoms should be cooled in each hyperfine state in order to reach the hydrodynamic regime in the degenerate quantum phase [22]. It is then important to focus upon the study of collisionless excitation spectra of these systems, seeking to improve the understanding of their low-temperature behavior, as well as the evolution between the collisionless and the hydrodynamic regimes, as increasing temperature suppresses Pauli blocking effects and enhances the collision rate. For this sake, in this work we derive a random-phase-approximation (RPA) description of the collective modes of two species of fermions in a harmonic well with mutual s-wave coupling at zero temperature, and we apply the formalism to the computation of density and spin fluctuations. This viewpoint is similar to the one adopted by Bruun [26] in a study of collective oscillations of trapped fermions subjected to attractive interactions, i.e., ^{6}Li. The paper is organized as follows. The specific RPA frame and the extraction of the elementary excitation spectrum of quasiparticles in a mean-field approach are discussed in Sec. II. Typical calculations of collective spectra for the lowest multipolarities are presented and discussed in Sec. III, while Sec. IV summarizes our main conclusions.

II. THE RANDOM-PHASE APPROXIMATION FOR A TRAPPED FERMION SYSTEM

We assume that the trapped atom system consists of non-interacting quasiparticles (QP's) in a mean field. Throughout this paper, this is referred to as the free system, which can be excited by an external field so that particle-hole (p-h) pairs involving, in principle, both hyperfine species (σ_1, σ_2) are created with energy Ω. The spectral properties of this non-homogeneous free system are contained in the free p-h propagator $G_0^{\sigma'\sigma}(\Omega)$, where the labels σ and σ' stand for either σ_1 or σ_2. Throughout this paper, the superscripts

$(\sigma_1\sigma_2)$ indicate a particle state $|\sigma_1\rangle$ and a hole state $|\sigma_2\rangle$.

We also suppose that a p-h effective interaction $V_{\text{p-h}}^{\sigma\sigma'}$ acting between the QP's gives rise to the dressed propagator for p-h pairs according to the RPA integral equation [27],

$$G^{\sigma'\sigma}(\Omega) = G_0^{\sigma'\sigma}(\Omega) + \sum_{\tau\tau'} G_0^{\sigma'\tau}(\Omega) V_{\text{p-h}}^{\tau\tau'} G^{\tau'\sigma}(\Omega). \tag{2.1}$$

It is worth noticing that the system under consideration is both nonhomogeneous [28–30] and polarized [31,32], so that the present development merges the corresponding formalisms as shown below. Hereafter, we consider longitudinal excitations involving propagation of p-h pairs of the same spin kind, created by spin-symmetric (s) and spin-antisymmetric (a) multipolar operators of the form

$$O_{s,a}^{\dagger} = \sum_{i=1}^{N_1} O_i^{\dagger} \pm \sum_{i=1}^{N_2} O_i^{\dagger} \tag{2.2}$$

with

$$O_i^{\dagger} = \begin{cases} r_i^l Y_{LM}(\theta_i,\phi_i), & L \neq 0 \\ r_i^2, & L = 0, \end{cases} \tag{2.3}$$

where N_1 (N_2) is the number of trapped atoms of species σ_1 (σ_2), and L is the multipolarity of the perturbation. Notice that a particle-particle interaction $V(\mathbf{r}-\mathbf{r}')$, with $\mathbf{r},\mathbf{r}'$, respectively, denoting particles with spin projections σ and σ', gives rise to a p-h interaction that scatters a p-h pair $(\sigma\sigma)$ at position $\mathbf{r}$ into a p-h pair $(\sigma'\sigma')$ at $\mathbf{r}'$, and that only collisions among different species are allowed. The free p-h propagators involved in longitudinal density fluctuations are diagonal in spin space and thus Eq. (2.1) splits into two equivalent systems of two equations each, intrinsic to polarized systems [31,32], which in a coordinate representation read

$$G^{\sigma\sigma}(\mathbf{r},\mathbf{r}') = G_0^{\sigma\sigma}(\mathbf{r},\mathbf{r}') + \int d^3r_1 d^3r_2 G_0^{\sigma\sigma'}(\mathbf{r},\mathbf{r}_1)$$
$$\times V_{\text{p-h}}^{\sigma\sigma'}(\mathbf{r_1},\mathbf{r}_2) G^{\sigma'\sigma}(\mathbf{r}_2,\mathbf{r}'),$$

$$G^{\sigma'\sigma}(\mathbf{r},\mathbf{r}')$$
$$= \int d^3r_1 d^3r_2 G_0^{\sigma'\sigma'}(\mathbf{r},\mathbf{r}_1) V_{\text{p-h}}^{\sigma'\sigma}(\mathbf{r}_1,\mathbf{r}_2) G^{\sigma\sigma}(\mathbf{r}_2,\mathbf{r}'). \tag{2.4}$$

In spatially inhomogeneous systems, it is convenient to expand both free and dressed propagators in multipolar decompositions [28,29],

$$G^{\sigma'\sigma}(\mathbf{r},\mathbf{r}',\Omega) = \sum_L G_L^{\sigma'\sigma}(r,r',\Omega) P_L(\hat{\mathbf{r}}\cdot\hat{\mathbf{r}}') \tag{2.5}$$

with the Legendre polynomials $P_L(x)$. The free p-h propagator reads

$$G_0^{\sigma\sigma}(\mathbf{r},\mathbf{r}',\Omega)$$
$$= \sum_{\nu\nu'} \phi_\nu^\sigma(\mathbf{r})[\phi_{\nu'}^\sigma(\mathbf{r})]^*[\phi_\nu^\sigma(\mathbf{r}')]^*\phi_{\nu'}^\sigma(\mathbf{r}')\chi_{\nu\nu'}^\sigma(\Omega), \tag{2.6}$$

where $\phi_\nu^\sigma(\mathbf{r})$ is a single-particle wave function for energy eigenvalue ε_ν^σ, and $\chi_{\nu\nu'}^\sigma$ is the generalized susceptibilities in terms of the Fermi-Dirac occupation numbers $n(\varepsilon)$,

$$\chi_{\nu\nu'}^\sigma = \frac{n(\varepsilon_\nu^\sigma) - n(\varepsilon_{\nu'}^\sigma)}{\Omega - (\varepsilon_{\nu'}^\sigma - \varepsilon_\nu^\sigma) + i\eta}. \tag{2.7}$$

Here the label ν stands for the spherical quantum numbers (nlm). The expressions for the multipole components $G_{0L}^{\sigma\sigma}(r,r',\Omega)$ are given in Appendix A.

Since Eq. (2.4) is a matrix equation calling for discretization in radial coordinates, it is convenient to map it onto a vector system for the transition densities defined as

$$\delta\rho_{LM}^{\sigma'\sigma}(\mathbf{r},\Omega) = \int d\mathbf{r}' G^{\sigma'\sigma}(\mathbf{r},\mathbf{r}',\Omega) r'^L Y_{LM}(\hat{\mathbf{r}}')$$
$$= \frac{4\pi}{2L+1} \delta\rho_L^{\sigma'\sigma}(r,\Omega) Y_{LM}(\hat{\mathbf{r}}), \tag{2.8}$$

where

$$\delta\rho_{LM}^{\sigma'\sigma}(r,\Omega) = \int dr' r'^{2+L} G_L^{\sigma'\sigma}(r,r',\Omega). \tag{2.9}$$

The multipolar susceptibility can then be computed as

$$\chi_{LM}^{\sigma'\sigma}(\Omega) = \int d\mathbf{r}\, r^L Y_{LM}^*(\hat{\mathbf{r}}) \delta\rho_{LM}^{\sigma'\sigma}(\mathbf{r},\Omega)$$
$$= \frac{4\pi}{2L+1} \int dr\, r^{2+L} \delta\rho_L^{\sigma'\sigma}(r,\Omega)$$
$$\equiv \chi_L^{\sigma'\sigma}(\Omega). \tag{2.10}$$

For dilute trapped systems at low temperature, we can reasonably represent the interaction potential by a contact interaction of the form $g\delta(\mathbf{r}-\mathbf{r}')$, where $g = 4\pi\hbar^2 a/m$ with m the mass and a the s-wave scattering length of the interacting atoms. Thus, we obtain from Eq. (2.4)

$$\delta\rho_L^{\sigma\sigma}(r,\Omega) = \delta\rho_{0L}^{\sigma\sigma}(r,\Omega)$$
$$+ \frac{4\pi g}{2L+1} \int dr' r'^2 G_{0L}^{\sigma\sigma}(r,r',\Omega) \delta\rho_L^{\sigma'\sigma}(r',\Omega),$$

$$\delta\rho_L^{\sigma'\sigma}(r,\Omega) = \frac{4\pi g}{2L+1} \int dr' r'^2 G_{0L}^{\sigma'\sigma'}(r,r',\Omega) \delta\rho_L^{\sigma\sigma}(r',\Omega). \tag{2.11}$$

Moreover, in view of Eq. (2.2), we shall consider the symmetric and antisymmetric density fluctuations for each atom species,

$$\delta\rho_\sigma^{(s,a)} = \frac{\delta\rho^{\sigma\sigma} \pm \delta\rho^{\sigma\sigma'}}{2}. \tag{2.12}$$

This representation enables us to distinguish what we hereafter call the density (symmetric) and spin (antisymmetric) fluctuations [33] as they usually appear in Fermi liquids. In fact, a multipolar operator $O_s^\dagger$ will likely generate a total density fluctuation proportional to $\delta\rho_\sigma^s + \delta\rho_{\sigma'}^s$, while out-of-phase perturbations produced by $O_a^\dagger$ will induce a spin fluctuation proportional to $\delta\rho_\sigma^a + \delta\rho_{\sigma'}^a$. In addition, this distinction enables one to analyze the influence of a given fluctuation on its own propagation, as well as on the oscillations in the other spin species.

The numerical procedure consists of solving the discretized equations (2.11) by matrix inversion, computing the susceptibilities (2.10), and constructing the total dynamic structure factors $S^{(s,a)} = -\mathrm{Im}\chi^{(s,a)}/\pi$ in both spin channels [31,32], where

$$\chi_L^{(s,a)} = \frac{1}{4}(\chi_L^{\sigma\sigma} + \chi_L^{\sigma'\sigma'} \pm \chi_L^{\sigma\sigma'} \pm \chi_L^{\sigma'\sigma}). \tag{2.13}$$

The collective spectrum of density and spin modes for a given multipolarity L is indicated by the poles of the real part of these responses, or corresponding peaks in the dynamical structure factors.

It is important to remark that this is a very general RPA description of collective excitations, valid for any system identified by its elementary excitations with single-particle spectrum ε_ν and states ϕ_ν, and by an effective p-h interaction $V_{p\text{-}h}$. In most applications to quantum liquids (see, for example, Refs. [29–32] and therein), one starts from a HF eigenspectrum and chooses the p-h coupling as the double functional derivative of the total energy with respect to the single-particle density. The HF spectrum of two hyperfine species of trapped fermions has been previously investigated in Ref. [7] for the case of an attractive coupling between the species, and in the present work we adopt the same philosophy for a repulsive interaction of strength g. The HF spectrum arises from the solution of the coupled nonlinear system in spherical coordinates,

$$\left\{ -\frac{\hbar^2}{2m}\frac{\partial^2}{\partial r^2} + \frac{\hbar^2 l(l+1)}{2mr^2} + \frac{m\omega_\sigma^2 r^2}{2} + g\rho_{\sigma'}(r) \right\} u_{nl}^\sigma(r)$$
$$= \varepsilon_{nl}^\sigma u_{nl}^\sigma(r) \tag{2.14}$$

for species $\sigma \neq \sigma'$, with partial densities

$$\rho_\sigma(r) = \sum_{nl}(2l+1)\frac{|u_{nl}^\sigma(r)|^2}{4\pi r^2}n(\varepsilon_{nl}^\sigma) \tag{2.15}$$

and trapping potentials $m\omega_\sigma^2 r^2/2$.

For vanishing temperature, the Fermi-Dirac occupation numbers are step functions limiting the summation to states below the respective Fermi sea ε_F^σ that fulfills the number equation $N_\sigma = \Sigma_\nu\Theta(\varepsilon_F^\sigma - \varepsilon_\nu^\sigma)$. In the forthcoming calculations, we shall consider both equal as well as different trap-

ping frequencies ω_σ for species 1 and 2, the latter case devised to take into account the corresponding magnetic projections of the trapped atoms, i.e., $(\omega_1/\omega_2)^2 = \sigma_1/\sigma_2$ [34].

III. CALCULATIONS AND RESULTS

We have solved the HF problem for variable numbers of ^{40}K atoms N_1, N_2 corresponding to different spin projections in an isotropic harmonic trap, with a mutual s-wave scattering length $a = 8.31$ nm [3]. As in Ref. [7], we start an iterative procedure from oscillator wave functions $u_{nl}^{osc}(r)$, and convergence is rapidly achieved. The self-consistent states are labeled by the same quantum numbers nl and the wave functions differ only slightly from the original ones. The low-energy states are the most sensitive to the size of the interaction strength, reaching deviations with respect to bare oscillator energies as large as 15%. The combinations of p-h states entering the free p-h propagator [see Eq. (A3)] are selected by angular momentum conservation, and we find that the elementary excitation energies in the denominators of the generalized susceptibilities [see Eq. (2.7)] are weakly spread around the noninteracting oscillator values.

A. Equal trapping potentials and populations

As a first step, we examine a trapped two-component Fermi gas with equal trapping potentials (ETP), i.e., $\omega_1 = \omega_2$, and the same number of atoms in each hyperfine level. Under these conditions, the RPA equations (2.4) can be decoupled for $\delta\rho_\sigma^{(s)}$ and $\delta\rho_\sigma^{(a)}$, giving rise to

$$\delta\rho^{(s,a)}(r) = \delta\rho_0^{(s,a)}(r)$$
$$\pm \frac{4\pi}{2L+1}g\int r'^2 G_{0\,L}(r,r',\Omega)\delta\rho^{(s,a)}(r'),$$
$$\tag{3.1}$$

where we identify $\delta\rho^{(s,a)} \equiv \delta\rho_\sigma^{(s,a)}$ and $G_{0\,L} \equiv G_{0\,L}^{\sigma\,\sigma}$ for either spin projection σ. Equations (3.1) are identical to the RPA equations for a *single*-component gas interacting through a repulsive (attractive) contact interaction, giving rise to the symmetric (antisymmetric) fluctuation.

In Fig. 1, we show the strengths $S^{(s,a)}$ of the monopolar ($L=0$) fluctuations for $N_{1,2} = 10^4$. It should be kept in mind that the spread of the peaks in $S^{(s,a)}(\Omega)$ is an artifact of the calculation, due to the introduction of the small numerical parameter η [cf. Eq. (2.7)]. The large-scale behavior of $S(\Omega)$ shows multiple excitations at energies close to $\Omega_n = \varepsilon_{n_1\,l} - \varepsilon_{n_2\,l} \approx 2\,n\,\omega_1$. These peaks decrease their amplitude (notice the logarithmic scale) as we increase the transferred energy. Although the s and a channels are different, we are not able to visualize them in the current scale. A narrow region around the oscillator excitation energy is displayed in the lower plot of Fig. 1. In fact, a careful analysis of the peaks indicates that they are grouped into two main sets. Only the strongly fragmented one around $\Omega = 2\omega_1$ can be viewed in this figure; the intensities in the second group lying at higher energies are too small in the current scale.
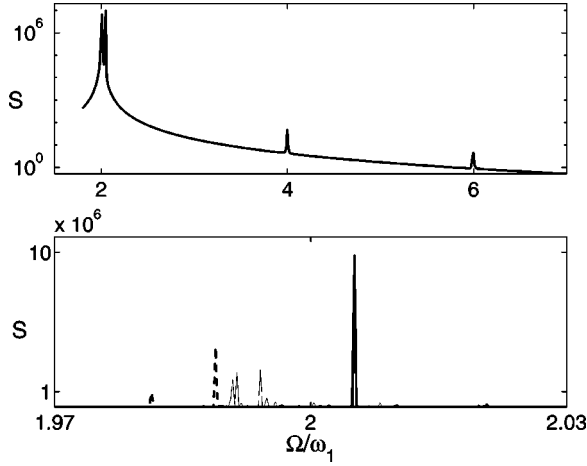
FIG. 1. Monopolar dynamic structure factor (in arbitrary units) in the ETP case for $N_1 = 10^4$ and $\omega_1 = 2\pi \times 70$ s^{-1}. The upper plot is depicted in a logarithmic scale and the lower one is a zoom of the main peak in a linear scale. The thin line corresponds to the HF p-h excitations, and thick and dashed lines indicate the RPA structure factor in the symmetric and antisymmetric channels, respectively.

Moreover, the spectra in both channels are clearly different: while the *s* channel is shifted upwards in energy, the *a* one lies at lower energies, in qualitative agreement with a simple model estimate sketched in Appendix B. It is important to mention that the QP's energies coming out from the HF calculation are such that the p-h excitation frequencies are lowered with respect to the oscillator ones by the mean-field interaction, while the p-h coupling introduced in the RPA formalism shifts the collective spectrum to higher energies.

The behavior of the dipolar fluctuation ($L=1$) is slightly different. Although both the *s* and *a* spectra are weakly fragmented, the amplitude of the oscillator mode at $\Omega = \omega_1$ is large. It is well known [35] that for equal trapping potentials and populations, there is a dipolar excitation in the symmetric channel, associated to the center-of-mass oscillation of the gas and occurring at the oscillator frequency. However, in the spin channel, this excitation appears at a slightly lower energy. These facts are verified in the present RPA calculation as shown in Fig. 2, where we see the dipolar structure
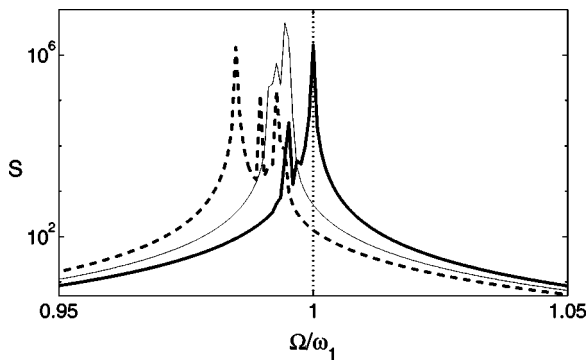
FIG. 2. Dipolar dynamic structure factor (in logarithmic scale and arbitrary units) for the same conditions as in Fig. 1. Thin, thick, and dashed lines correspond to the HF system, symmetric, and antisymmetric channels, respectively.
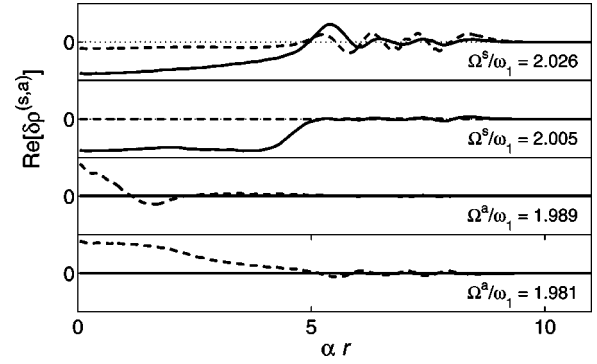
FIG. 3. Monopolar density fluctuations for equal trapping potentials and populations (in arbitrary units) with $N_{1,2} = 10^4$. Solid and dashed lines correspond to density and spin excitations, respectively, at the poles of each channel. α^{-1} is the distance unit for the trapping potential of species 1, $\alpha^{-1} = \sqrt{m\omega_1/\hbar} \approx 0.53 \ \mu$m^{-1}.

factor for $N_1 = N_2 = 10^4$ atoms. We can also observe that in addition to these modes, fragmented poles of a collective nature show up as indicated by the simple model in Appendix B.

In addition, we have numerically verified that the position of the main peaks can be accounted for by the analytical sum-rule formula derived by Vichi and Stringari [21]. In particular, for $N_{1,2} = 10^4$, we obtain the sum-rule energies $\Omega_{SR} \approx 2.0043\omega_1, 0.9840\omega_1$, and $1.9914\omega_1$ for $L = 0(s), 1(a)$, and $2(s)$, respectively, while the corresponding RPA results are $\Omega_{RPA} = 2.0051\omega_1$, $0.9848\omega_1$, and $1.9920\omega_1$.

Let us now examine the spatial profiles of the density fluctuations. In principle, one would expect that if the system is excited with a given operator *s* or *a* [cf. Eq. (2.2)] in the vicinity of a peak in one of these channels, a density fluctuation will develop that reflects both the character of the external field and the nature of the intrinsic excitation of the free system. As an illustration, in Fig. 3 we show the real parts of the monopolar density oscillations for the same conditions as in Fig. 1 at the frequencies given by the poles of the response. We observe that when the symmetric fluctuation is important within the bulk of the trapped system, the antisymmetric counterpart is completely negligible and vice versa. However, at the energy of the pole in the symmetric channel ($\Omega^s \approx 2.03$), surface oscillations develop both in $\delta\rho^s$ and $\delta\rho^a$; this behavior can be attributed to the proximity of a weak peak in the antisymmetric structure factor (not visible in the scale of Fig. 1).

B. Unequal potential wells and populations

In the recent experimental achievement of DeMarco and Jin [4], ^{40}K atoms in two magnetic sublevels $|F = \frac{9}{2}, m_F = \frac{7}{2}\rangle$ (type 1 atoms) and $|F = \frac{9}{2}, m_F = \frac{9}{2}\rangle$ (type 2 atoms) were confined and cooled. Although the ratio $\omega_2/\omega_1 = (\sigma_2/\sigma_1)^{1/2} \approx 1.13$ is very close to unity, we take it into account as an explicit feature of the real nonsymmetric configuration. We also consider unequal populations ranging from $\Delta = N_2/N_1 \approx 0.3$ to $\Delta \approx 3$, which can be built during the evaporative cooling process.
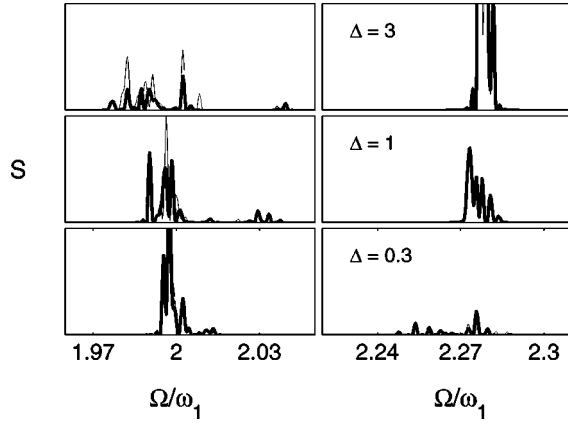
FIG. 4. Dynamic structure factor for $L=0$ (in arbitrary units) for the symmetric channel of the interacting and free system with $N_1 = 10^4$ and several concentrations, in thick and thin lines, respectively. Each column display a different range in the energy scale.

As in the ETP case, we analyze the dynamic structure factors and the fluctuations created by multipolar external fields. In Fig. 4, we show the symmetric dynamic structure factor for several values of the population ratio Δ, $N_1 = 10^4$ and a monopolar excitation. The structure of spin fluctuations cannot be distinguished from the density ones within the scale of this plot. The essential features of the response can be summarized as follows. (i) In either channel, the strength of each p-h transition is redistributed so that the structure factor is fragmented around the noninteracting peaks with some intensity appearing at higher energies. (ii) For low or high values of Δ, the structure of the most populated species essentially reproduces the pattern of the noninteracting quasiparticles, while the spectrum of the other species is highly fragmented with a largely suppressed amplitude. (iii) Given either species, as the number of atoms in the other spin projection increases, the complementary excitation appears displaying considerable fragmentation.

We have also made calculations for multipolar excitations with $L=1,2$; in Figs. 5 and 6, we show the corresponding results for the structure factor. In general, the description of the monopolar excitation applies as well to higher multipolarities, however we can mention some differences: the dipolar peaks are narrower and fragmentation seems to be stron-
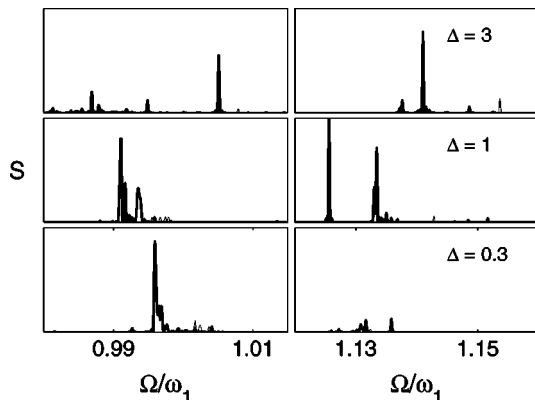
FIG. 5. Same as Fig. 4 for the dipolar dynamic structure factor.
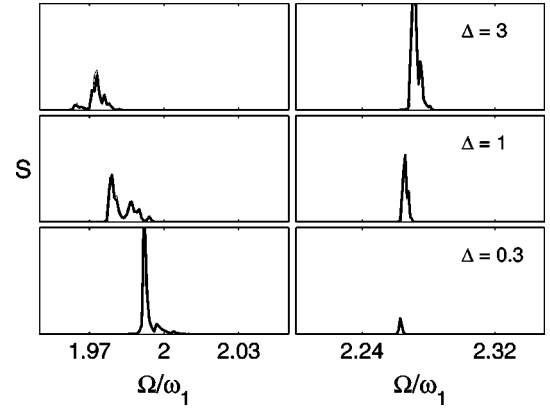
FIG. 6. Same as Fig. 4 for the quadrupolar dynamic structure factor.

ger. In particular, in the equal population case ($\Delta = 1$) there exist well-resolved fragmented peaks as intense as the original HF ones.

The real parts of the monopolar transition densities are displayed in Fig. 7. The s and a density profiles for each component have been scaled to a common value at a given frequency. This is a convenient criterion, since if one depicts the four profiles in the same scale, near the intrinsic p-h frequencies of each component the complementary density fluctuation appears largely depleted. Before analyzing the fluctuation profiles, we want to call attention to the shape of the HF equilibrium density profiles. In Table I, we quote, as a function of Δ, some shape parameters related to the spheri-
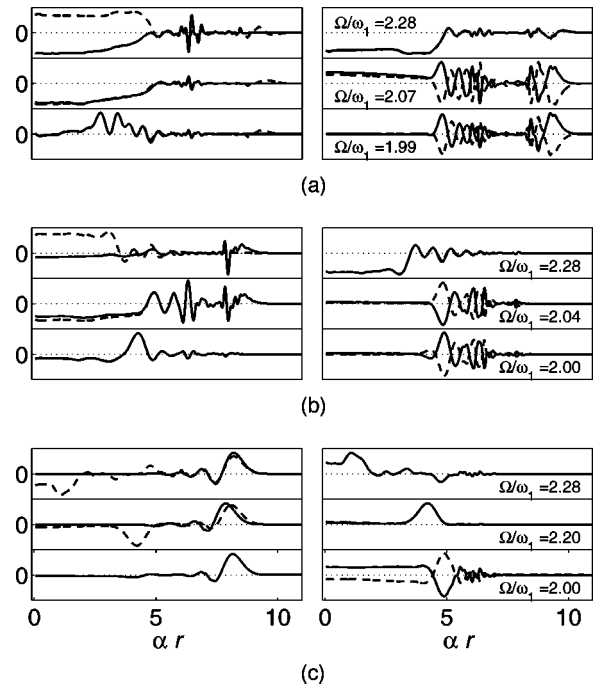
FIG. 7. Monopolar density fluctuations (in arbitrary units) for $N_1 = 10^4$. The upper, middle, and lower plots correspond to $\Delta = 3,1,0.3$, respectively, for $\sigma_1 = \frac{7}{2}$ (left column) and $\sigma_2 = \frac{9}{2}$ (right column). Solid and dashed lines indicate $\delta\rho_\sigma^{(s)}$ and $\delta\rho_\sigma^{(a)}$, respectively.

TABLE I. Shape parameters related to the HF probability density profiles $P_\sigma(r)$ (see text) for $N_1 = 10^4$ and several concentrations. All distances are given in harmonic-oscillator units $\alpha^{-1} = (\hbar/m\omega_1)^{1/2} \approx 1.9 \ \mu$m.

Parameter	$\Delta = 0.3$		$\Delta = 1$		$\Delta = 3$	
	σ_1	σ_2	σ_1	σ_2	σ_1	σ_2
$P_{\max}$	0.017	0.022	0.017	0.018	0.017	0.015
$\alpha R_{\max}$	5.64	4.28	5.64	5.24	5.64	6.28
αR_{edge}	8.71	6.59	8.75	8.17	8.79	9.86
FWHM	5.04	3.92	5.04	4.72	4.96	5.68

cal probability density distribution $P_\sigma(r)$ defined as

$$P_\sigma(r) = \frac{r^2 \rho_\sigma(r)}{N_\sigma}. \tag{3.2}$$

Particularly, we list the maximum probability $P_{\max}$ (which is attained at $R_{\max}$), the location of the density edge R_{edge}, and the full width at half maximum (FWHM) of the probability distribution. These parameters will help us to understand the main aspects of the excitation profiles.

In Fig. 7, we show some typical monopolar density fluctuations for each spin component at the lowest-lying collective peaks and several concentrations. We observe that as we increase Δ (from bottom to top in Fig. 7), both fluctuations $\delta\rho_2^{(s,a)}$ for a given frequency extend beyond the ρ_2 edge. As an illustration, let us consider in detail the case $\Delta = 0.3$. For the excitation with $\Omega \approx 2\omega_1$, $\delta\rho_2^{(s,a)}$ is bounded to roughly the size of the density of σ_2 atoms ($\alpha r \lesssim 7$, $\alpha^2 = m\omega_1/\hbar$) while $\delta\rho_1^{(s,a)}$ extends far beyond this cutoff, within the ρ_1 range. For small Δ, the corrections $\delta\rho^{1\,2}$ are unimportant, in general, due to the relatively weak coupling of the σ_1 species to the few σ_2 atoms. However, in the same limit $\delta\rho^{2\,2}$ acquires important corrections $\delta\rho^{2\,1}$, essentially driven by the large number of σ_1 atoms. We also see two different behaviors related to the Ω dependence: for frequencies close to $2\omega_1$, $\delta\rho_2^{(s)}$ and $\delta\rho_2^{(a)}$ present opposite signs, revealing that the induced contribution $\delta\rho^{2\,1}$ is larger than the intrinsic one $\delta\rho^{2\,2}$. In fact, if the system is excited with frequencies close to $2\omega_1$, large $\delta\rho_1$ fluctuations should be expected, which in turn introduce, through the $V_{\text{p-h}}$ interaction, sizeable $\delta\rho^{2\,1}$ contributions to $\delta\rho_2^{(s,a)}$. In turn, exciting at $\Omega \approx 2\omega_2$ creates $\delta\rho^{2\,2}$, thus the correction to $\delta\rho^{2\,1}$ is second order in the interaction and the s and a fluctuations are the same. On the other hand, as ρ_1 extends beyond ρ_2, a stimulus acting at $\Omega = 2\omega_2$ induces a cross fluctuation $\delta\rho^{12}$ inside the bulk of the type 1 system, i.e., at smaller radii (cf. Fig. 7).

As one increases the number of particles in species 2, their density profiles extend farther (see Table I) and there are few noticeable changes in the spatial localization of the excitation. However, in general, close to $2\omega_2$ we find a strong induced fluctuation $\delta\rho^{12}$ in the spatial region where $P_2(r)$ is larger than $P_1(r)$ and correspondingly for $\delta\rho^{21}$ near $2\omega_1$. If one keeps increasing Δ, the perturbative interpretation is no longer valid for every multipole and species. For

$\Delta = 3$, the fluctuations occupy a broader region, roughly from $\alpha r = 4$ to $\alpha r = 10$, which can be attributed to a wider ρ_2 density.

In addition to the vanishing at the origin of the $L \neq 0$ fluctuation, the main difference between the spatial profiles of distinct multipolarities lies in an enhanced symmetry of the channels for $L = 2$. In this case, we have observed that the cross fluctuation of a given component is non-negligible *only* near the free p-h transition of its counterpart, suggesting a weaker p-h effective interaction for higher multipolarities [cf. Eq. (2.11)].

Another feature to mention is the difference from the ETP case. In that situation, we have the same spatial fluctuations for either spin projection and well-defined channels s and a; however, in this more general problem, we observe different spatial profiles for each component and mixed behaviors within the channels, i.e., given a pole in the symmetric susceptibility, fluctuations may exhibit similar amplitudes in both channels.

IV. DISCUSSION AND SUMMARY

In this work, we have developed a RPA formalism for a two-species, trapped Fermi gas at vanishing temperature, which may provide guidelines to current experimental research. We have shown that the interspecies interaction gives rise to a fragmented zero sound spectrum. We analyzed both the equal trapping potential and populations, as well as a general case with unequal potentials and populations intended to mimic an experimental situation. The main differences arise in the spectra; while in the ETP case the poles associated to density and spin fluctuations were clearly distinct, in the general case these fluctuations cannot be disentangled. The density and spin responses of the system share the same energy spectrum, however with unequal amplitudes. For the excitation with $L = 1$, we have found in the density channel and for the ETP case a pole at the bare oscillator frequency corresponding to rigid oscillation of the system; however, this is no longer true for a more realistic configuration with unequal trapping frequencies. Although we checked that the eigensolutions of Eq. (2.14) differ only by a few percent from the bare oscillator basis functions, we cannot prevent propagation of small errors in the response calculation, which ought to be safely computed out of the true HF wave functions at the expense of an increase in computing time. Finally, we should mention that this two-component RPA formalism may be straightforwardly generalized to nonzero temperatures by taking into account the finite temperature Fermi-Dirac occupation numbers.

APPENDIX A:

To evaluate the free p-h propagator, we use the 3D harmonic-oscillator basis for each spin projection:

$$\phi_{nlm}^{\sigma}(\mathbf{r}) = A_{nl}^{\sigma} \exp(-\alpha_{\sigma}^2 r^2/2) r^l L_n^{l+1/2}(\alpha_{\sigma}^2 r^2) Y_{lm}(\hat{\mathbf{r}})$$

$$\equiv R_{nl}(r) Y_{lm}(\hat{\mathbf{r}}), \tag{A1}$$

where $\alpha_{\sigma}^2 = m\omega_{\sigma}/\hbar$, Y_{lm} are the spherical harmonic functions, $L_n^{l+1/2}$ are the generalized Laguerre functions, and A_{nl}^{σ} a normalization constant. The multipolar component $G_{0L}^{\sigma\sigma}$ reads

$$G_{0L}^{\sigma\sigma}(r,r',\Omega) = \frac{1}{(4\pi)^2} \sum_{nl,n'l'} (2l+1)(2l'+1)$$

$$\times (R_{nl}R_{n'l'})(r)(R_{nl}R_{n'l'})(r')$$

$$\times |\langle l0l'0|L0\rangle|^2 \chi_{nl,n'l'}(\Omega). \tag{A2}$$

In order to compute the elementary susceptibilities $\chi_{nl,n'l'}$ in Eq. (A2), we have used the HF energies extracted from Eq. (2.14) instead of the bare harmonic-oscillator ones. Further simplifications arise from the properties of the Clebsch-Gordan coefficients and HO wave functions $R_{nl}(r)$; in particular, explicit expressions for monopolar, dipolar, and quadropolar excitations ($L=0,1,2$) can be written. The monopolar free p-h propagator reads

$$G_{00}^{\sigma\sigma}(r,r',\Omega) = \frac{1}{(4\pi)^2} \sum_{nln'} (2l+1)R_{nl}(r)R_{n'l}(r)$$

$$\times R_{nl}(r')R_{n'l}(r)\chi_{nl,n'l}(\Omega). \tag{A3}$$

In this case, we use the excitation operator $O_i^{\dagger} = r_i^2$; this yields the following noninteracting susceptibility:

$$\chi_{00}^{\sigma\sigma} = \frac{1}{\alpha_{\sigma}^2} \sum_{nl} (2l+1)[\chi_{nl,n-1l}n(n+l+1/2)$$

$$+ \chi_{nl,n+1l}(n+1)(n+l+3/2)], \tag{A4}$$

which in the case of a large enough number of particles, zero temperature, and HO energies can be simplified to yield

$$S_{00}^{\sigma}(\Omega) = -\frac{1}{\pi} \text{Im}[\chi_0^{\sigma\sigma}] \approx \frac{1}{\alpha_{\sigma}^2} \frac{3N_{\sigma}}{4} (6N_{\sigma})^{1/3} \delta(\Omega - 2\omega_{\sigma}). \tag{A5}$$

Similarly, the dipolar propagator can be written as

$$G_{01}^{\sigma\sigma}(\Omega) = \frac{3}{(4\pi)^2} \sum_{nln'} [(l+1)R_{nl}(r)R_{n'l+1}(r)R_{nl}(r')$$

$$\times R_{nl+1}(r')\chi_{nl,n'l+1}(\Omega)$$

$$+ lR_{nl}(r)R_{nl-1}(r)R_{nl}(r')$$

$$\times R_{nl-1}(r')\chi_{nl,n'l-1}(\Omega)] \tag{A6}$$

yielding a temperature-independent free response

$$\chi_{01}^{\sigma\sigma} = \frac{1}{\alpha_{\sigma}^2} \frac{3N_{\sigma}}{8\pi} \left(\frac{1}{\Omega - \omega_{\sigma} + i\eta} - \frac{1}{\Omega + \omega_{\sigma} + i\eta} \right) \tag{A7}$$

with a $T=0$ structure factor

$$S_{01}^{\sigma} = \frac{1}{\alpha_{\sigma}^2} \frac{3N_{\sigma}}{8\pi} \delta(\Omega - \omega_{\sigma}). \tag{A8}$$

APPENDIX B: A SIMPLIFIED MODEL FOR ZERO SOUND MODES

In order to get a basic understanding of the different excitations of the two-component gas, we propose a very simple model for the noninteracting propagator that allows for illustrative analytical results. Let us assume that each of the coexisting species possesses only one elementary excitation with energy ω_{σ} ($\omega_{\sigma'}$). The corresponding free propagator reads

$$G_0^{\sigma\sigma}(\mathbf{r},\mathbf{r'}) = F^{\sigma}(\mathbf{r})[F^{\sigma}(\mathbf{r'})]^* \left(\frac{1}{\omega - \omega_{\sigma} + i\eta} - \frac{1}{\omega + \omega_{\sigma} + i\eta} \right), \tag{B1}$$

where $F^{\sigma}(\mathbf{r})$ is the wave function of the excited p-h pair at the given position. Replacement of Eq. (B1) into the RPA system of equations (2.4) brings into evidence that these propagators are of the form

$$G^{\sigma\sigma}(\mathbf{r},\mathbf{r'}) = F^{\sigma}(\mathbf{r})\chi_0^{\sigma}[\Gamma^{\sigma\sigma}(\mathbf{r'})]^*,$$

$$G^{\sigma'\sigma}(\mathbf{r},\mathbf{r'}) = gF^{\sigma'}(\mathbf{r})\chi_0^{\sigma'}[\Gamma^{\sigma'\sigma}(\mathbf{r'})]^*, \tag{B2}$$

where in turn

$$\Gamma^{\sigma\sigma} = F^{\sigma\sigma} + \tilde{g}^* \chi_0^{\sigma'} \Gamma^{\sigma'\sigma},$$

$$\Gamma^{\sigma'\sigma} = \tilde{g}^* \chi_0^{\sigma} \Gamma^{\sigma\sigma} \tag{B3}$$

represent dressed p-h wave functions, which depend on the p-h interaction strength

$$\tilde{g} = g \int d\mathbf{x}[F^{\sigma}(\mathbf{x})]^* F^{\sigma'}(\mathbf{x}) \equiv \langle \sigma\sigma|V_{\text{p-h}}|\sigma'\sigma'\rangle. \tag{B4}$$

The system (B3) possesses a simple algebraic solution, from which we can write the dynamical susceptibilities

$$\chi^{\sigma\sigma} = \frac{\chi_0^{\sigma}|\theta^{\sigma}|^2}{D},$$

$$\chi^{\sigma'\sigma} = \tilde{g}\frac{\chi_0^{\sigma}\chi_0^{\sigma'}[\theta^{\sigma}]^*\theta^{\sigma'}}{D}, \tag{B5}$$

where

$$D(\omega) = 1 - |\tilde{g}|^2 \chi_0^{\sigma}(\omega)\chi_0^{\sigma'}(\omega) \tag{B6}$$

and $\theta^{\sigma} = \int d\mathbf{r}_i O_i^{\dagger} F^{\sigma}(\mathbf{r}_i)$ is the matrix element of the transition operator.

The appearance of the common denominator $D(\omega)$ in Eqs. (B5) reflects the fact that the RPA describes collective fluctuations of the system as a whole. The zeros of D in Eq. (B6) can be easily found to be

$$\omega_0^2 = \frac{\omega_\sigma^2 + \omega_{\sigma'}^2}{2} \pm \left| \frac{\omega_\sigma^2 - \omega_{\sigma'}^2}{2} \right| \left[1 + \frac{16|\tilde{g}|^2 \omega_\sigma \omega_{\sigma'}}{(\omega_\sigma^2 - \omega_{\sigma'}^2)^2} \right]^{1/2} .$$

(B7)

The evolution of the collective modes with interaction strength is encompassed in Eq. (B7); for $\omega_\sigma = \omega_{\sigma'}$ and assuming a small relative strength $|\tilde{g}|/\omega_\sigma$, the dispersion relation of the modes illustrates the fragmentation of the elementary excitation into two collective states with energies

$$\omega_0 = \omega_\sigma \pm |\tilde{g}|.$$

(B8)

The corresponding form of the total spin symmetric and antisymmetric responses can be shown to be [cf. Eq. (2.13)]

$$\chi^{(s,a)} = \frac{1}{4} \sum_{\sigma = \sigma_1, \sigma_2} \frac{\chi_0^\sigma |\theta^\sigma|^2}{2(1 \pm \tilde{g} \chi_0^\sigma)}$$

(B9)

(for real $\tilde{g}$). It is important to remark that although both frequencies (B8) correspond to poles of Eq. *each* term in (B9), explicit computation shows that $\omega_\sigma + |\tilde{g}|$ has zero amplitude in the antisymmetric response while $\omega_\sigma - |\tilde{g}|$ has zero amplitude in the symmetric one. The higher and lower frequencies in Eq. (B8) can then be attributed to the symmetric and antisymmetric fluctuations, respectively.

[1] F.S. Cataliotti, E.A. Cornell, C. Fort, M. Inguscio, F. Marin, M. Predevelli, L. Ricci, and G.M. Tino, Phys. Rev. A **57**, 1136 (1998); M. Prevedelli, F.S. Cataliotti, E.A. Cornell, J.R. Ensher, C. Fort, L. Ricci, G.M. Tino, and M. Inguscio, *ibid.* **59**, 886 (1999).

[2] W.I. McAlexander, E.R.I. Abraham, N.W.M. Ritchie, C.J. Williams, H.T.C. Stoof, and R.G. Hulet, Phys. Rev. A **51**, R871 (1995); M.O. Mewes, G. Ferrari, F. Schreck, A. Sinatra, and Ch. Salomon, *ibid.* **61**, 011403 (2000).

[3] B. DeMarco, J.L. Bohn, J.P. Burke, Jr., M. Holland, and D.S. Jin, Phys. Rev. Lett. **82**, 4208 (1999).

[4] B. DeMarco and D.S. Jin, Science **285**, 1703 (1999).

[5] D.A. Butts and A.S. Rokhsar, Phys. Rev. A **55**, 4346 (1997).

[6] J. Schneider and H. Wallis, Phys. Rev. A **57**, 1253 (1998).

[7] G.M. Bruun and K. Burnett, Phys. Rev. A **58**, 2427 (1998).

[8] K. Mølmer, Phys. Rev. Lett. **80**, 1804 (1998).

[9] M. Amoruso, A. Minguzzi, S. Stringari, M.P. Tosi, and L. Vichi, Eur. Phys. J. D **4**, 261 (1998).

[10] L. Vichi, M. Inguscio, S. Stringari, and G.M. Tino, J. Phys. B **31**, L899 (1998).

[11] L. Vichi, M. Amoruso, A. Minguzzi, S. Stringari, and M.P. Tosi, Eur. Phys. J. D **11**, 335 (2000).

[12] L. Viverit, C.J. Pethick, and H. Smith, Phys. Rev. A **61**, 053605 (2000).

[13] A. Minguzzi and M. P. Tosi, Phys. Lett. A **268**, 142 (2000).

[14] H.T.C. Stoof, M. Houbiers, C.A. Sackett, and R.G. Hulet, Phys. Rev. Lett. **76**, 10 (1996).

[15] M. Houbiers, R. Ferwerda, H.T.C. Stoof, W.I. McAlexander, C.A. Sackett, and R.G. Hulet, Phys. Rev. A **56**, 4864 (1997).

[16] M.A. Baranov and D.S. Petrov, Phys. Rev. A **58**, R801 (1998).

[17] G. Bruun, Y. Castin, R. Dum, and K. Burnett, Eur. Phys. J. D **7**, 433 (1999).

[18] M.A. Baranov, JETP Lett. **70**, 396 (1999).

[19] W. Zhang, C.A. Sackett, and R.G. Hulet, Phys. Rev. A **60**, 504 (1999).

[20] S.K. Yip and Tin-Lun Ho, Phys. Rev. A **59**, 4653 (1999).

[21] L. Vichi and S. Stringari, Phys. Rev. A **60**, 4734 (1999).

[22] G.M. Bruun and C.W. Clark, Phys. Rev. Lett. **83**, 5415 (1999).

[23] M. Amoruso, J. Meccoli, A. Minguzzi, and M.P. Tosi, Eur. Phys. J. D **7**, 441 (1999).

[24] M. Amoruso, J. Meccoli, A. Minguzzi, and M.P. Tosi, Eur. Phys. J. D **8**, 361 (2000).

[25] B. DeMarco, S.B. Papp, and D.S. Jin, e-print cond-mat/0101445 (2001).

[26] G.M. Bruun, e-print cond-mat/0012364.

[27] A. Fetter and D. Walecka, *Quantum Theory of Many Particle Systems* (McGraw-Hill, New York, 1971).

[28] G. Bertsch and S.F. Tsai, Phys. Rep. **18**, 125 (1975).

[29] M. Casas and S. Stringari, J. Low Temp. Phys. **79**, 135 (1990).

[30] M. M. Calbi and E. S. Hernández, J. Low Temp. Phys. **120**, 1 (2000).

[31] E.S. Hernández, J. Navarro, and A. Polls, Phys. Lett. B **413**, 1 (1997); Nucl. Phys. A **627**, 460 (1997).

[32] S.M. Gatica, E.S. Hernández, and J. Navarro, Phys. Rev. B **60**, 15 302 (1999).

[33] D. Pines and P. Nozières, *The Theory of Quantum Liquids* (Addison-Wesley, Redwood City, CA, 1990), Vol. II.

[34] W. Ketterle, D. S. Durfee, and D. M. Stamper-Kurn, in *Bose-Einstein Condensation of Atomic Gases*, edited by M. Inguscio, S. Stringari, and C. E. Wieman (IOS Press, Amsterdam, 1999).

[35] W. Kohn, Phys. Rev. **123**, 1242 (1961).